Q. J. R. Meteorol. Soc. (2005), **131**, pp. 1759–1782 doi: 10.1256/qj.04.101

A new dynamical core for the Met Office's global and regional modelling of the atmosphere

By T. DAVIES*, M. J. P. CULLEN, A. J. MALCOLM, M. H. MAWSON, A. STANIFORTH, A. A. WHITE and N. WOOD
Met Office, Exeter, UK

(Received 1 July 2004; revised 22 November 2004)

SUMMARY

A computational scheme suitable for numerical weather prediction and climate modelling over a wide range of length scales is described. Its formulation is non-hydrostatic and fully compressible, and shallow atmosphere approximations are not made. Semi-implicit, semi-Lagrangian time-integration methods are used. The scheme forms the dynamical core of the unified model used at the Met Office for all its operational numerical weather prediction and in its climate studies.

KEYWORDS: Climate modelling Deep atmosphere Fully compressible Non-hydrostatic NWP Predictor–corrector Semi-implicit Semi-Lagrangian

1. INTRODUCTION

For more than a decade, a unified model (UM) has been used at the Met Office for both low resolution climate modelling and high resolution operational numerical weather prediction (NWP). The split-explicit dynamical formulation for the hydrostatic model introduced in the early 1990s was described by Cullen and Davies (1991). The UM system is regularly upgraded to provide a better service in NWP and climate modelling, and as a result the quality of both has improved significantly. (For example, in terms of root mean square error of mean-sea-level pressure, the skill of the 72-hour forecast today is equivalent to that of the 24-hour forecast 15 years ago.) This paper describes a major upgrade to the dynamical core which was successfully introduced into operations for NWP in 2002 and in climate change studies from 2004.

The outline and justification of the proposed new scheme were presented by Cullen *et al.* (1997), together with tests of some of its components. Inevitably, as a result of experience during the pre-implementation phase, some modifications were made; also, further practical and theoretical evidence for the adopted choices came to light. We argue for, and give an account of, the scheme as implemented in the UM during 2002. Its main features are:

- non-hydrostatic, fully compressible, deep-atmosphere formulation using a terrain-following, height-based vertical coordinate;
- discretization using a horizontally staggered Arakawa C-grid and a vertically staggered Charney–Phillips grid;
- semi-Lagrangian (SL) advection for all prognostic variables, except density, with conservative and monotone treatment of tracers;
- Eulerian treatment of the continuity equation for mass conservation;
- predictor–corrector implementation of a two-time-level (2TL), semi-implicit (SI) time integration scheme;
- three-dimensional iterative solution of a variable-coefficient elliptic equation for the pressure increment at each time step.

In addition to upgrading the core numerical techniques, some of the design choices were made to allow better coupling with both the physical parametrizations and the

* Corresponding author, present address: JCMM Meteorology Building, The University of Reading, PO Box 243, Reading, RG6 6BB, UK. e-mail: terry.davies@metoffice.gov.uk

data assimilation. Improved geostrophic adjustment properties are an important element in improving this coupling. The UM remains a grid-point model on a latitude–longitude grid. This facilitates running a limited-area model (LAM) with the same code.

To present all the details of the scheme would result in too lengthy a paper. Instead, we aim here to give a brief description of the main features. Full documentation is available as an internal Met Office report (see Staniforth *et al.* (2004)).

Section 2 outlines the rationale behind the design of the scheme. It is followed by a summary of the equations (section 3) and by details of the grids used (section 4). The time integration scheme and the solution of the discretized equations are then outlined in sections 5 and 6 respectively. Section 7 presents sample validations conducted with various configurations of the model and indicates the current level of performance. Conclusions are presented in section 8.

2. Design strategy and rationale

In choosing which continuous equations to discretize, our strategy has been to avoid unnecessary approximations. Accordingly, the fully compressible, non-hydrostatic equations are used, without the shallow atmosphere approximation (although the spherical geopotential approximation—see Gill (1982), p. 92—remains).

The use of a fully compressible and non-hydrostatic formulation means that sound waves have to be considered, but SI time integration methods introduced by Robert (1969) neutralize this computational disadvantage without compromising the treatment of the motions important in weather forecasting and climate modelling (Tapp and White 1976; Cullen 1990; Tanguay *et al.* 1990). Regarding compressibility, Davies *et al.* (2003) concluded that no model, at least of a height-coordinate form, which filters sound waves is likely to be acceptably accurate for NWP at all relevant scales. Lions *et al.* (1992a,b) show that relaxing the hydrostatic assumption improves the nonlinear behaviour of the equations, and Oliger and Sundström (1978) show that the boundary value problem for LAM applications is ill-posed with any specification of local, pointwise boundary conditions if the hydrostatic approximation is used. The case for using the deep-atmosphere equations is discussed by White and Bromley (1995) and White *et al.* (2005), and primarily amounts to the desirability of retaining a complete representation of the Coriolis force.

When the new scheme was developed, the only available formulation of the fully compressible equations which maintained global conservation properties and did not involve additional approximations used height-based coordinates. More recent work suggests that mass-based coordinates would also be viable (Wood and Staniforth 2003). Also, when the scheme was designed, it seemed that only SI methods where a linear Helmholtz equation had to be solved would be cost-effective in an operational context. This constrained the options considered. More recently, Côté *et al.* (1998) and Cullen (2001) have shown that more-implicit methods may indeed be advantageous.

In the regimes where the model is to be used, the ratio of wind speed to the speed of sound is small. In this case, the limiting small-scale behaviour is anelastic, which means that the evolution equation for density reduces (in this asymptotic limit) to a diagnostic local mass-balance constraint. If SI methods are used to treat the sound waves, then use of an *Eulerian* flux-form scheme for the evolution equation for the density does indeed lead to this diagnostic local constraint in the asymptotic, small-scale limit. Hence, the scheme uses an Eulerian flux form for the continuity equation, which gives the additional benefit of exact mass conservation. While use of this Eulerian form in conjunction with semi-Lagrangian forms of the other prognostic equations (see below) allows a weak

instability away from the anelastic limit, the formulation has proved sufficiently stable for practical purposes.

The scheme is also optimized for balanced flow in the sense that it embodies an accurate scheme for a balanced model in the appropriate asymptotic limit (see Cullen (1999)). The horizontal latitude–longitude grid is C-grid staggered because this arrangement has the best geostrophic adjustment properties overall for atmospheric flows (Arakawa and Lamb 1977). It has also tended to work better than other staggerings with SI time-schemes. The vertical grid uses the Charney–Phillips staggering. For first-order averaging and differencing, this arrangement avoids the computational mode of the Lorenz staggering and thus gives better balanced structures (Arakawa and Konor 1996). For the same reasons, the C-grid and the Charney–Phillips vertical staggering are better at representing the dispersion properties of gravity waves; see, for example, Thuburn *et al.* (2002). In solving a (semi-) geostrophic adjustment problem in a vertical slice, Cullen (1989) found satisfactory solutions only when Charney–Phillips staggering was used. In addition, it was necessary at each time step to solve an elliptic equation with flow-dependent coefficients in order to derive the ageostrophic flow. Guided by this experience, our scheme in this paper used a predictor–corrector approach to obtain an elliptic pressure correction equation at each time step. Having chosen a solution procedure that results in a three-dimensional, variable-coefficient, second-order, partial differential equation to solve, then using the full (i.e. unapproximated) non-hydrostatic equations of motion does not significantly increase the computational cost of the model.

SL advection schemes are being used successfully by many NWP groups—see e.g. Staniforth and Côté (1991), Bates *et al.* (1993), Ritchie *et al.* (1995) and Côté *et al.* (1998). In combination with SI time stepping, SL schemes permit the use of much longer time steps (Robert 1981; Tanguay *et al.* 1990; Golding 1992). (Explicit Eulerian advection time steps are generally limited by the maximum velocity anywhere in the domain, which means in practice that the time step is governed by a tiny percentage of the flow.) To ensure that initially positive quantities remain positive and spurious negative values are not produced, the monotone constraint of Bermejo and Staniforth (1992) is applied. SL schemes to date have generally been non-conservative but in long-term climate integrations, conservation of mass and of species in the absence of sources and sinks is considered important. The use of an Eulerian treatment of the continuity equation in this scheme, together with the conservation constraint of Priestley (1993) in the SL advection, ensures dry mass conservation and improves species conservation.

The model is designed to be used without explicit representation of diffusion. On large scales, atmospheric flow can be considered as energy-conserving except in the boundary layer, and in areas of deep convection or mountains (Cullen *et al.* 1987). In such regions, the required dissipation and energy exchange are provided in the model by the physical parametrizations. On small scales, the use of monotone advection schemes provides a flow-dependent dissipation which has been shown in several studies to give realistic results; see, for instance, the review by Fureby and Grinstein (2002). However, operation without explicit representation of diffusion is a design ideal: as noted in later sections, selective smoothing is needed in practice to overcome specific numerical difficulties.

3. Governing equations

The prognostic variables are the three-dimensional wind $\mathbf{u}$ with components (u, v, w), potential temperature θ, Exner pressure Π, dry density ρ_{dry} and mixing ratios of moist quantities. Mixing ratios are defined as $m_X = \rho_X/\rho_{\mathrm{dry}}$ for any quantity X such

as the various phases of water. If present, aerosols or chemical species are treated as mixing ratios but they will not be discussed further. ρ is the density and subscripts 'dry', 'vap', 'cl', and 'cf' signify dry air, water vapour, cloud water and cloud ice respectively. The density ρ of moist air is thus given by

$$\rho = \rho_{\text{dry}}\left(1 + \sum_{X=\text{vap,cl,cf}} m_X\right). \tag{3.1}$$

Exner pressure is defined as $\Pi = (p/p_0)^\kappa$, where p is pressure and $p_0 = 10^5$ Pa is a reference pressure. $\kappa \equiv R_{\text{dry}}/c_p$ where R_{dry} is the gas constant for dry air and c_p is the specific heat at constant pressure for dry air (the 'dry' subscripts for κ and c_p are omitted since only the dry forms are used here). Potential temperature is $\theta \equiv T/\Pi$, where T is temperature and, where moist effects need to be taken into account, the virtual potential temperature is $\theta_{\text{v}} \equiv T_{\text{v}}/\Pi$, where

$$T_{\text{v}} = T\left(\frac{1 + m_{\text{vap}}/\varepsilon}{1 + \sum_{X=\text{vap,cl,cf}} m_X}\right), \tag{3.2}$$

and $\varepsilon \equiv R_{\text{dry}}/R_{\text{vap}}$ ($\cong 0.622$).

The equations of motion used for the wind components (u, v, w) are the non-hydrostatic equations for a deep atmosphere in spherical polar coordinates (λ, ϕ, r) with origin at the Earth's centre. λ is the longitude, ϕ the latitude and r is the radius. (See Gill (1982) pages 91–94 for a discussion of the coordinate system.) These equations are:

$$\frac{\text{D}u}{\text{D}t} - f_r v + f_\phi w - \frac{uv\tan\phi}{r} + \frac{uw}{r} + \frac{c_p\theta_{\text{v}}}{r\cos\phi}\frac{\partial\Pi}{\partial\lambda} = P^u, \tag{3.3}$$

$$\frac{\text{D}v}{\text{D}t} + f_r u - f_\lambda w + \frac{u^2\tan\phi}{r} + \frac{vw}{r} + \frac{c_p\theta_{\text{v}}}{r}\frac{\partial\Pi}{\partial\phi} = P^v, \tag{3.4}$$

$$\frac{\text{D}w}{\text{D}t} - f_\phi u + f_\lambda v - \frac{(u^2+v^2)}{r} + g + c_p\theta_{\text{v}}\frac{\partial\Pi}{\partial r} = P^w, \tag{3.5}$$

where the P terms are the tendencies from the physics parametrizations and for most applications P^w is set to zero. The material derivative is given by

$$\frac{\text{D}}{\text{D}t} \equiv \frac{\partial}{\partial t} + \frac{u}{r\cos\phi}\frac{\partial}{\partial\lambda} + \frac{v}{r}\frac{\partial}{\partial\phi} + w\frac{\partial}{\partial r}. \tag{3.6}$$

When the coordinate poles are coincident with the geographical poles, the Coriolis terms are $(f_\lambda, f_\phi, f_r) = (0, 2\Omega\cos\phi, 2\Omega\sin\phi)$, where Ω is the Earth's angular speed of rotation. However, the equations are written for a general grid where the coordinate poles need not be coincident with the geographical poles. In the LAM context, this has the advantage that the computational grid can be rotated so that its equator lies within the LAM domain, thus leading to a more uniform horizontal grid. The resulting Coriolis terms are given in appendix A.

The internal energy equation and the transport equations take the form

$$\frac{\text{D}X}{\text{D}t} = P^X, \tag{3.7}$$

where X represents any of potential temperature, moisture mixing ratios, and other included variables such as aerosols or chemical species. The continuity equation (conservation of dry mass) is

$$\frac{\partial\rho_{\text{dry}}}{\partial t} + \nabla\cdot(\rho_{\text{dry}}\mathbf{u}) = 0. \tag{3.8}$$

The equation of state ($p = R_{\text{dry}}\rho T_{\text{v}}$) is written as

$$\kappa \Pi \theta_{\text{v}} \rho = \frac{p}{c_p}. \tag{3.9}$$

4. Grids and staggering

The horizontal grid is regular in longitude λ and latitude ϕ. The variables are Arakawa C-grid staggered (Arakawa and Lamb 1977) but with the scalar variables held at the poles. Although this means that u is held at the poles, it is not truly prognostic there but is diagnosed from v at the latitude immediately surrounding a pole (see e.g. appendix B of McDonald and Bates (1989)).

In NWP and climate modelling it is standard practice to use terrain-following coordinates for ease in applying lower boundary conditions (Phillips 1957) but to gradually flatten the coordinate surfaces so that at upper levels they become horizontal (Simmons and Burridge 1981). The same approach is taken here but in a height-based system. Introducing z, the height above mean sea level, the vertical coordinate η is normalized so that $\eta = 0$ at $z = h(\lambda, \phi)$, where $h(\lambda, \phi)$ is the height of the orography above $r = a$ (a is the Earth's mean radius), and $\eta = 1$ at $z = z_{\text{T}}$, where z_{T} is the fixed height of the model lid. When $h = 0$ (e.g. everywhere over the ocean) η is given simply by $\eta = z/z_{\text{T}}$. When $h > 0$ there is a choice to be made as to how to specify the flattening. Let $\eta = \eta_{\text{I}}$ be the level at and above which the coordinate is flat and look for a function $F(\eta)$ such that $z = \eta z_{\text{T}} + F(\eta)$, $0 \le \eta \le \eta_{\text{I}}$, and which satisfies the lower boundary condition $F(0) = h$ together with the constraints that $F(\eta_{\text{I}}) = 0$ at the interface and $\partial z/\partial \eta$ is continuous across the interface, i.e. $\partial F/\partial \eta = 0$ at $\eta = \eta_{\text{I}}$. These conditions are satisfied by any polynomial $F(\eta) = h(1 - \eta/\eta_{\text{I}})^p$ of order $p > 1$. Choosing $p = 2$ leads to the following relationship between η and z:

$$z = \begin{cases} \eta z_{\text{T}} + h\left(1 - \dfrac{\eta}{\eta_{\text{I}}}\right)^2, & 0 \le \eta < \eta_{\text{I}} \\ \eta z_{\text{T}}, & \eta_{\text{I}} \le \eta \le 1. \end{cases} \tag{4.1}$$

Since the same number of levels must fit into $z_{\text{I}} - h$, vertical resolution increases with h. Furthermore, since $\partial z/\partial \eta > 0$, z_{I} must satisfy $z_{\text{I}} > 2h$.

The vertical grid spacing in η is chosen to be irregular since it is desirable to have higher resolution near the surface where there are large vertical gradients and fluxes. To reduce truncation errors the grid structure has an underlying functional form. Kálnay de Rivas (1972) showed that any smooth function will give a second-order-accurate approximation to both the first and second derivatives. A quadratic function is chosen for smoothness and to give higher resolution near the lower boundary. η at level k is given by $\eta_k = (k/N)^2$ where N is the total number of vertical levels. The ratio of the thickness of successive levels is $(2k + 1)/(2k - 1)$ which decreases as k increases. However, it is desirable to have the layers thicken more quickly (but gradually) towards the model top so as to place the lid well above any feature whose fidelity is considered important. It also helps to reduce any reflection from the upper boundary of vertically propagating waves. Thus, the quadratic nature of the underlying grid is only used up to a suitable height from where an imposed gradual thickening of the layers is applied by choosing $\eta_{k+1} = \eta_k + \beta_k(\eta_k - \eta_{k-1})$ where $\beta_k > 1$ is a factor which increases as k increases (typically $1.025 < \beta_k < 1.1$). Once the η values and z_{T} have been chosen, z at every point can be found using (4.1).

In this terrain-following coordinate system, the horizontal derivatives in the pressure-gradient term become

$$\left.\frac{\partial \Pi}{\partial \chi}\right|_r = \left(\frac{\partial \Pi}{\partial \chi} - \frac{\partial \Pi}{\partial r}\frac{\partial r}{\partial \chi}\right)_\eta , \tag{4.2}$$

where χ represents λ or ϕ and the subscripts denote the surfaces that are held constant during the differentiation. The material derivative then takes the form

$$\frac{\mathrm{D}}{\mathrm{D}t} \equiv \left.\frac{\partial}{\partial t}\right|_\eta + \left.\frac{u}{r\cos\phi}\frac{\partial}{\partial \lambda}\right|_\eta + \left.\frac{v}{r}\frac{\partial}{\partial \phi}\right|_\eta + \dot{\eta}\frac{\partial}{\partial \eta}. \tag{4.3}$$

The continuity equation (3.8) becomes

$$\frac{\partial}{\partial t}\left(r^2\rho_{\mathrm{dry}}\frac{\partial r}{\partial \eta}\right) + \frac{1}{\cos\phi}\frac{\partial}{\partial \lambda}\left(r^2\rho_{\mathrm{dry}}\frac{\partial r}{\partial \eta}\frac{u}{r}\right) + \frac{1}{\cos\phi}\frac{\partial}{\partial \phi}\left(r^2\rho_{\mathrm{dry}}\frac{\partial r}{\partial \eta}\frac{v\cos\phi}{r}\right) + \frac{\partial}{\partial \eta}\left(r^2\rho_{\mathrm{dry}}\frac{\partial r}{\partial \eta}\dot{\eta}\right) = 0. \tag{4.4}$$

In the vertical a Charney–Phillips staggering is used. θ and w are held on the same levels ('θ-levels') including the upper boundary where $w = 0$. However, θ is not used at the lower boundary $z = 0$ (see the end of this section). u, v, ρ and Π are held on the intermediate levels ('ρ-levels'). The grid is set for 'θ-levels' using (4.1) and the 'ρ-levels' are currently placed halfway between. The vertical grid is therefore irregular. However, as 'ρ-levels' are at mid-points, differencing and averaging operators to 'ρ-levels' are second-order accurate. All other vertical averages and differences are formally only first-order accurate, albeit close to second-order due to the slow variation in the vertical spacing.

The main drawback of the Charney–Phillips staggering is the need for a temperature variable in the pressure gradient term for the horizontal winds. For all but the lowest wind levels this is effectively supplied through vertical averaging. At the lowest level such averaging would use a surface value which usually would not produce an appropriate temperature due to the large near-surface gradients (for idealized, inviscid flow it would be appropriate). Using the parametrizations to obtain the desired temperature or carrying temperature at the first wind level would result in normal-mode behaviour more like the Lorenz staggering, so neither is appropriate. Instead, the method chosen here is not to carry a prognostic temperature variable at the surface (apart from the skin temperature) but to assume that the lowest-layer potential temperature is non-varying with height, i.e. isentropic. In normal use, this layer is at most 20 m thick and for the model with complete physics it appears to be a suitable way of obtaining the temperature at the lowest layer (typically at 10 m or less). The moisture variables and any tracers are also assumed to be non-varying with height within the lowest layer. For inviscid problems where the lowest layer is not isentropic this is a source of error which can be reduced by making the lowest layer thinner.

The natural mass-conserving upper and lower boundary conditions are $\dot{\eta} = 0$ at $\eta = 0$ and $\eta = 1$. Equivalent conditions on w are required since w is a dependent variable. At the top of the domain the coordinate surface is horizontal and so $\dot{\eta} = 0$ corresponds to $w = 0$. At the surface $\eta = 0$, $w = 0$ is again applied since when physical processes are active a no-slip condition is appropriate.

5. AN OVERVIEW OF THE TIME INTEGRATION SCHEME

For clarity, this and the following section describe only the adiabatic part of the scheme. Consider a prognostic equation of the form

$$\frac{\mathrm{D}\mathbf{X}(\mathbf{x}, t)}{\mathrm{D}t} = \mathbf{L}(\mathbf{x}, t, \mathbf{X}) + \mathbf{N}(\mathbf{x}, t, \mathbf{X}), \tag{5.1}$$

where $\mathbf{x}$ denotes position, $\mathbf{X}$ represents any of the prognostic variables (m_X, θ, u, v, w), $\mathbf{L}$ represents terms linear in $\mathbf{X}$, and $\mathbf{N}$ represents terms nonlinear in $\mathbf{X}$. Note that for some of the prognostic variables some of the right-hand side (r.h.s.) terms may be zero. The basic 2TL SI SL scheme applied to (5.1) may be written as

$$\frac{\mathbf{X}^{n+1} - \mathbf{X}^n_{\mathrm{d}}}{\Delta t} = \alpha(\mathbf{L} + \mathbf{N})^{n+1} + (1 - \alpha)(\mathbf{L} + \mathbf{N})^n_{\mathrm{d}}, \tag{5.2}$$

where n is the time-level, Δt the time step, subscript 'd' denotes evaluation at the departure point $\mathbf{x}_{\mathrm{d}}$ and α is a time-weighting coefficient. The scheme is formally second-order accurate in time if $\alpha = 1/2$. If $\alpha > 1/2$ (referred to as off-centring) then the scheme is damping. It was shown in Cullen (1999) that selective off-centring can drive the solution towards that of an appropriate simplified model, which may be beneficial in enabling the model to adjust to non-smooth inputs from physical parametrizations or when the model is used for data assimilation. (5.2) may be rearranged as

$$\mathbf{X}^{n+1} - \alpha\Delta t\mathbf{L}^{n+1} = [\mathbf{X} + (1 - \alpha)\Delta t(\mathbf{L} + \mathbf{N})]^n_{\mathrm{d}} + \alpha\Delta t\mathbf{N}^{n+1}. \tag{5.3}$$

An equation of this generic form needs to be solved for each prognostic variable. In general the r.h.s. terms at time-level $n + 1$ may depend upon some or all of the prognostic variables and this implicit coupling of the set of equations means that they cannot easily be solved. The general approach is to reduce the implicit nonlinear coupling in some way and then derive an elliptic boundary-value problem.

Two alternative treatments of the nonlinear terms are either to extrapolate them to time-level $n + \frac{1}{2}$ (McDonald and Bates 1989; Bates *et al.* 1993; Temperton *et al.* 2001) or to evaluate them at the latest available time-level and iterate (Côté *et al.* 1998; Cullen 2001; Yeh *et al.* 2002). Neither of these is used here. Instead, a predictor–corrector scheme is used. In the predictor step, wherever time-level $n + 1$ terms are required in the target SL scheme (5.3), time-level n values are used instead. These are replaced in the corrector step by better estimates. The resulting scheme may be written symbolically as:

$$\mathbf{X}^{(1)} = \mathbf{X}^n_{\mathrm{d}} + (1 - \alpha)\Delta t(\mathbf{L} + \mathbf{N})^n_{\mathrm{d}} + \alpha\Delta t(\mathbf{L} + \mathbf{N})^n, \tag{5.4}$$

$$\mathbf{X}^{(2)} - \alpha\Delta t\mathbf{L}^{(2)} = \mathbf{X}^{(1)} + \alpha\Delta t(\mathbf{N}^{(1)} - \mathbf{N}^n - \mathbf{L}^n), \tag{5.5}$$

where the numbered superscripts in brackets denote successive estimates of $\mathbf{X}$. (5.4) represents the predictor step and (5.5) the corrector step. Summing (5.4) and (5.5) results in

$$\mathbf{X}^{(2)} - \alpha\Delta t\mathbf{L}^{(2)} = [\mathbf{X} + (1 - \alpha)\Delta t(\mathbf{L} + \mathbf{N})]^n_{\mathrm{d}} + \alpha\Delta t\mathbf{N}^{(1)}, \tag{5.6}$$

an approximation of (5.3), where $\mathbf{X}^{(2)}$ can be considered to be $\mathbf{X}^{n+1}$, the state vector at time-level $n + 1$.

For the predictor step, the SL scheme as in (5.4) is applied to m_X, θ, u, v and w. Exact correction equations would involve adding back all the appropriate time-level $n + 1$ terms and subtracting the time-level n terms that were used in their place in the

prediction step. To avoid the coupled implicit system of equations that would result, only some of the time-level $n+1$ terms are used. For other terms, values for time-level $n+1$, estimated from known values, are used to reduce the implicit coupling. The continuity equation for the dry density ρ_{dry} is used in SI Eulerian flux form so that dry mass is conserved. Further details of the scheme are given below.

The SL advection adopted here is similar to that described in Bates *et al.* (1993) and many of the details regarding interpolation and location of the departure points are as in that paper. The scheme has been coded to allow for different orders of interpolation up to quintic Lagrange. In general, higher order is preferred for accuracy but is computationally expensive. Interpolations to departure points are normally cubic but for moisture variables quintic interpolation is used in the vertical for global configurations to prevent the tropical lower stratosphere from becoming too dry.

The winds used to compute the trajectories for the advection in (5.4) are the time-extrapolated values

$$\mathbf{u}^{n+\frac{1}{2}} = \tfrac{3}{2}\mathbf{u}^{n} - \tfrac{1}{2}\mathbf{u}^{n-1}. \tag{5.7}$$

In the spatially discretized versions of (5.4) and (5.5), given in the following section, the time weight (or off-centring parameter) α assumes four different values, α_i, $i = 1, 2, 3, 4$, which allows terms responsible for different modes of behaviour to be off-centred independently. The weights α_1 and α_3 are mainly associated with inertio-gravity modes and at low resolution the values $\alpha_1 = \alpha_3 = 0.6$ can be used. However, at the resolutions used in operational NWP, noise can develop in very strong jets and this is eliminated by setting $\alpha_1 = \alpha_3 = 0.7$. The weights α_2 and α_4 are mainly associated with acoustic modes which do not need to be treated accurately and so the values $\alpha_2 = \alpha_4 = 1$ are used.

6. The discretized equations and solution algorithm

(*a*) *Notation*

The differencing operator is defined as $\delta_{Nx} X_k \equiv (X_{k+N/2} - X_{k-N/2})/(x_{k+N/2} - x_{k-N/2})$ where N is an integer and k is an index. For regular grid spacing this is second-order accurate but for irregular grids (e.g. in the vertical) it reduces to first order. The time-averaging operator is defined as $\overline{X}^{\alpha} \equiv (1-\alpha)X^{n} + \alpha X^{n+1}$ where α is the time-weighting. When $\alpha = 1/2$ the averaging is second-order accurate but only first-order accurate otherwise. The horizontal averaging operator is defined as $\overline{X}_i^{\chi} \equiv (X_{i+\frac{1}{2}} + X_{i-\frac{1}{2}})/2$ where χ represents λ or ϕ. The vertical averaging operator is defined as

$$\overline{X}_k^{\chi} \equiv \{(\chi_k - \chi_{k-\frac{1}{2}})X_{k+\frac{1}{2}} + (\chi_{k+\frac{1}{2}} - \chi_k)X_{k-\frac{1}{2}}\}/(\chi_{k+\frac{1}{2}} - \chi_{k-\frac{1}{2}}),$$

where χ represents η or r. Henceforth, for clarity, the superscript n is omitted from time-level n variables.

(*b*) *Details of the discretizations*

(5.4) and (5.5) are the simplified symbolic representation of the SI SL discretization applied in the model. In the following sections the actual form of these equations used for each type of prognostic variable handled in an SL manner is given, together with the Eulerian discretization of the density equation and the linearized form of the equation of state.

(i) *Moisture variables and passive tracers.* For moisture variables, m_X, as well as all passive tracers, the operators $\mathbf{L}$ and $\mathbf{N}$ are identically zero. Then, the combination of (5.4) and (5.5), i.e. (5.6), reduces to

$$m_X^{(2)} = m_X^{(1)} = (m_X)_{\mathrm{d}}. \tag{6.1}$$

(ii) *Potential temperature.* Since the operators $\mathbf{L}$ and $\mathbf{N}$ are identically zero also for the potential temperature, θ, this variable could in principle be handled in the same way as for the moisture variables. However, problems were encountered during early development of the model due to the large basic-state gradient of potential temperature. As a result a 'non-interpolating in the vertical' approach is taken. In this approach the departure point, $\mathbf{x}_{\mathrm{d}}$, is projected in the vertical onto the nearest model level giving the position $\mathbf{x}_{\mathrm{dl}}$. Then, noting that $\mathbf{x}_{\mathrm{d}}$–$\mathbf{x}_{\mathrm{dl}}$ is aligned with the vertical, the value of θ_{d} is estimated as

$$\theta_{\mathrm{d}} \approx \theta_{\mathrm{dl}} - \Delta t (w - w^*) \frac{\partial \theta}{\partial r}, \tag{6.2}$$

where w^* is the vertical velocity required to move a parcel from the departure point r_{dl} to the arrival point r_{a} in one time step, given by

$$w^* \equiv (r_{\mathrm{a}} - r_{\mathrm{dl}})/\Delta t, \tag{6.3}$$

and the subscript 'dl' indicates horizontal interpolation to $\mathbf{x}_{\mathrm{dl}}$. The term $-\Delta t(w - w^*)\partial\theta/\partial r$ is then treated similarly to $\mathbf{L} + \mathbf{N}$ in (5.4)–(5.5), with evaluation at $\mathbf{x}_{\mathrm{d}}$ replaced by evaluation at $\mathbf{x}_{\mathrm{dl}}$. Thus, the first predictor for θ is given by

$$\theta^{(1)} = \theta_{\mathrm{dl}} - (1 - \alpha_2)\Delta t[(w - w^*)\delta_{2r}\theta]_{\mathrm{dl}} - \alpha_2 \Delta t (w - w^*)\delta_{2r}\theta. \tag{6.4}$$

However, before going to the corrector stage, a second predictor for θ is obtained which is written as

$$\theta^{(1\mathrm{a})} = \theta_{\mathrm{dl}} - (1 - \alpha_2)\Delta t[(w - w^*)\delta_{2r}\theta]_{\mathrm{dl}} - \alpha_2 \Delta t (w - w^*)\delta_{2r}\theta^{(1)}. \tag{6.5}$$

This is the same as (6.4) except that θ in the final term of (6.4) has been replaced by the first predictor $\theta^{(1)}$.

The correction equation for θ has a form similar to that of (5.5) and is given by

$$\theta^{(2)} = \theta^{(1\mathrm{a})} - \alpha_2 \Delta t (w^{(2)} - w^*)\delta_{2r}\theta_{\mathrm{ref}} + \alpha_2 \Delta t (w - w^*)\delta_{2r}\theta_{\mathrm{ref}}, \tag{6.6}$$

where $w^{(2)}$ is an estimate for w^{n+1} defined in (6.13) and

$$\delta_{2r}\theta_{\mathrm{ref}} = \max\left[\delta_{2r}\theta^{(1\mathrm{a})}, \left(\frac{1 - G_{\mathrm{tol}}}{\alpha_2\alpha_4\Delta t^2 c_p \delta_r \Pi}\right)\left(\frac{1 + \sum_{X=\mathrm{vap,cl,cf}} m_X^{(2)}}{1 + m_{\mathrm{vap}}^{(2)}/\varepsilon}\right)\right]. \tag{6.7}$$

The justification for applying a limit to $\delta_{2r}\theta^{(1\mathrm{a})}$ and the form for G_{tol} are given later in this section.

(iii) *The wind components.* The predictors for the wind components, corresponding to (5.4), are given by:

$$\begin{aligned} u^{(1)} = {} & u_{\mathrm{d}} - (1 - \alpha_4)\Delta t (\overline{w}^{\lambda r} f_\phi)_{\mathrm{d}} \\ & + (1 - \alpha_3)\Delta t \left\{ \overline{v}^{\lambda\phi} f_r - \frac{c_p}{\overline{r}^{\lambda}\cos\phi}\left(\overline{\theta_{\mathrm{v}}}^{\lambda r}\delta_\lambda \Pi - \overline{\theta_{\mathrm{v}}\delta_r\Pi}^{\lambda r}\delta_\lambda r\right)\right\}_{\mathrm{d}} \\ & - \alpha_4 \Delta t (\overline{w}^{\lambda r} f_\phi) + \alpha_3 \Delta t \left\{ \overline{v}^{\lambda\phi} f_r - \frac{c_p}{\overline{r}^{\lambda}\cos\phi}\left(\overline{\theta_{\mathrm{v}}}^{\lambda r}\delta_\lambda \Pi - \overline{\theta_{\mathrm{v}}\delta_r\Pi}^{\lambda r}\delta_\lambda r\right)\right\}, \end{aligned} \tag{6.8}$$

$$v^{(1)} = v_{\mathrm{d}} + (1-\alpha_4)\Delta t(\overline{w}^{\phi r} f_\lambda)_{\mathrm{d}} - (1-\alpha_3)\Delta t \left\{ \overline{u}^{\lambda\phi} f_r + \frac{c_p}{\overline{r}^{\phi}} \left(\overline{\theta}_{\mathrm{v}}^{\phi r} \delta_\phi \Pi - \overline{\theta_{\mathrm{v}} \delta_r \Pi}^{\phi r} \delta_\phi r \right) \right\}_{\mathrm{d}} + \alpha_4 \Delta t(\overline{w}^{\phi r} f_\lambda) - \alpha_3 \Delta t \left\{ \overline{u}^{\lambda\phi} f_r + \frac{c_p}{\overline{r}^{\phi}} \left(\overline{\theta}_{\mathrm{v}}^{\phi r} \delta_\phi \Pi - \overline{\theta_{\mathrm{v}} \delta_r \Pi}^{\phi r} \delta_\phi r \right) \right\}, \tag{6.9}$$

$$w^{(1)} = w_{\mathrm{d}} + (1-\alpha_4)\Delta t(f_\phi \overline{u}^{\lambda r} - f_\lambda \overline{v}^{\phi r} - g - c_p \theta_{\mathrm{v}} \delta_r \Pi)_{\mathrm{d}} + \alpha_4 \Delta t(f_\phi \overline{u}^{\lambda r} - f_\lambda \overline{v}^{\phi r} - g - c_p \theta_{\mathrm{v}} \delta_r \Pi). \tag{6.10}$$

To obtain expressions for the correctors for u, v and w, corresponding to (5.5), nonlinear terms of the general form $\theta^{(2)} \nabla \Pi^{(2)}$ need to be handled (where $\Pi^{(2)} \equiv \Pi^{n+1}$). In the horizontal momentum equations this is achieved by replacing $\theta^{(2)}$ by $\theta^{(1\mathrm{a})}$ so that $\theta^{(2)} \nabla_{\mathrm{h}} \Pi^{(2)} \simeq \theta^{(1\mathrm{a})} \nabla_{\mathrm{h}} \Pi^{(2)}$ where ∇_{h} represents the horizontal gradient operator. The accuracy of the horizontal momentum equations therefore depends upon $\theta^{(1\mathrm{a})}$ being a good estimate for $\theta^{(2)}$. In the vertical momentum equation the nonlinear term is approximated by using the identity

$$\theta^{(2)} \delta_r \Pi^{(2)} \equiv \theta^{(1\mathrm{a})} \delta_r (\Pi^{(2)} - \Pi) + \theta^{(2)} \delta_r \Pi + (\theta^{(2)} - \theta^{(1\mathrm{a})}) \delta_r (\Pi^{(2)} - \Pi),$$

and then neglecting the term $(\theta^{(2)} - \theta^{(1\mathrm{a})}) \delta_r (\Pi^{(2)} - \Pi)$ which is small if either $\theta^{(1\mathrm{a})}$ is a good estimate for $\theta^{(2)}$ or if $\delta_r \Pi$ is a good estimate for $\delta_r \Pi^{(2)}$. Thus, $\theta^{(2)} \delta_r \Pi^{(2)} \simeq \theta^{(2)} \delta_r \Pi + \theta^{(1\mathrm{a})} \delta_r (\Pi^{(2)} - \Pi)$.

The equations for the corrected velocity components are then

$$u^{(2)} = u^{(1)} - \alpha_3 \Delta t \frac{c_p}{\overline{r}^{\lambda} \cos\phi} \left\{ \overline{(\theta_{\mathrm{v}}^{(1\mathrm{a})} - \theta_{\mathrm{v}})}^{r\lambda} \delta_\lambda \Pi - \overline{(\theta_{\mathrm{v}}^{(1\mathrm{a})} - \theta_{\mathrm{v}}) \delta_r \Pi}^{r\lambda} \delta_\lambda r \right\} + \alpha_3 \Delta t f_r \overline{(v^{(2)} - v)}^{\lambda\phi} - \alpha_3 \Delta t \frac{c_p}{r \cos\phi} \times \left\{ \overline{\theta_{\mathrm{v}}^{(1\mathrm{a})}}^{r\lambda} \delta_\lambda (\Pi^{(2)} - \Pi) - \overline{\theta_{\mathrm{v}}^{(1\mathrm{a})} \delta_r (\Pi^{(2)} - \Pi)}^{r\lambda} \delta_\lambda r \right\}, \tag{6.11}$$

$$v^{(2)} = v^{(1)} - \alpha_3 \Delta t \frac{c_p}{\overline{r}^{\phi}} \left\{ \overline{(\theta_{\mathrm{v}}^{(1\mathrm{a})} - \theta_{\mathrm{v}})}^{r\phi} \delta_\phi \Pi - \overline{(\theta_{\mathrm{v}}^{(1\mathrm{a})} - \theta_{\mathrm{v}}) \delta_r \Pi}^{r\phi} \delta_\phi r \right\} - \alpha_3 \Delta t f_r \overline{(u^{(2)} - u)}^{\lambda\phi} - \alpha_3 \Delta t \frac{c_p}{r} \times \left\{ \overline{\theta_{\mathrm{v}}^{(1\mathrm{a})}}^{r\phi} \delta_\phi (\Pi^{(2)} - \Pi) - \overline{\theta_{\mathrm{v}}^{(1\mathrm{a})} \delta_r (\Pi^{(2)} - \Pi)}^{r\phi} \delta_\phi r \right\}, \tag{6.12}$$

and

$$G w^{(2)} = w^{(1)} - (1-G) w - \alpha_4 \Delta t c_p (\theta_{\mathrm{v}}^{(1\mathrm{a})} - \theta_{\mathrm{v}}) \delta_r \Pi - \alpha_4 \Delta t c_p \theta_{\mathrm{v}}^{(1\mathrm{a})} \delta_r (\Pi^{(2)} - \Pi), \tag{6.13}$$

where

$$G = 1 - \alpha_2 \alpha_4 \Delta t^2 c_p \left(\frac{1 + m_{\mathrm{vap}}^{(2)}/\varepsilon}{1 + \sum_{X=\mathrm{vap,cl,cf}} m_X^{(2)}} \right) \delta_{2r} \theta_{\mathrm{ref}} \delta_r \Pi, \tag{6.14}$$

and $\theta_{\rm v}^{(1a)}$ is the virtual potential temperature which is evaluated from (3.2), together with $\theta_{\rm v} \equiv T_{\rm v}/\Pi$, using $\theta^{(1a)}$ and $m_X^{(2)}$ as estimates for θ and m_X. In deriving (6.14), (6.6) has been used to eliminate $\theta^{(2)}$ in favour of $w^{(2)}$, and hence the appearance of $\delta_{2r}\theta_{\rm ref}$.

(iv) *Dry density.* As noted in section 2, the equation for the dry density, $\rho_{\rm dry}$, is handled in a semi-implicit, flux-form Eulerian manner and is:

$$\rho_{\rm dry}^{(2)} = \rho_{\rm dry} - \frac{\Delta t}{r^2\delta_\eta r}\left[\frac{1}{\cos\phi}\delta_\lambda\left(\frac{\overline{r^2\rho_{\rm dry}\delta_\eta r}^{\lambda}}{\overline{r}^{\lambda}}\overline{u}^{\alpha_1}\right) + \frac{1}{\cos\phi}\delta_\phi\left(\frac{\overline{r^2\rho_{\rm dry}\delta_\eta r}^{\phi}}{\overline{r}^{\phi}}\overline{v}^{\alpha_1}\cos\phi\right) - \delta_\eta\left\{\overline{r^2\rho_{\rm dry}}^{r}\left(\frac{\overline{\overline{u}^{\eta}}^{\lambda}}{\overline{r}^{\lambda}\cos\phi}\delta_\lambda r + \frac{\overline{\overline{v}^{\eta}}^{\phi}}{\overline{r}^{\phi}}\delta_\phi r\right)^{\alpha_1}\right\} + \delta_\eta\left(\overline{r^2\rho_{\rm dry}}^{r}\overline{w}^{\alpha_2}\right)\right]. \quad (6.15)$$

Note that where $\rho_{\rm dry}$ appears on the r.h.s. of (6.15), it is evaluated at time-level n in order to avoid making the discretization more implicit. In the δ_η term, the identity

$$\dot\eta \equiv \frac{1}{\delta_\eta r}\left(w - \frac{\overline{\overline{u}^{\eta}}^{\lambda}}{\overline{r}^{\lambda}\cos\phi}\delta_\lambda r - \frac{\overline{\overline{v}^{\eta}}^{\phi}}{\overline{r}^{\phi}}\delta_\phi r\right) \quad (6.16)$$

has been used. No further changes are made to $\rho_{\rm dry}^{(2)}$ and therefore $\rho_{\rm dry}^{n+1} \equiv \rho_{\rm dry}^{(2)}$.

(v) *Equation of state.* The equation of state (3.9) is assumed to hold for the latest estimators for each variable (denoted by superscript (2)), i.e.

$$\kappa\Pi^{(2)}\theta_{\rm v}^{(2)}\rho^{(2)} = \frac{p^{(2)}}{c_p}, \quad (6.17)$$

where $p^{(2)}$ is the value of pressure given by $p^{(2)} \equiv p_0(\Pi^{(2)})^{1/\kappa}$. Defining primed quantities to denote differences between time-level n values and the latest estimators, i.e. $\Pi' \equiv \Pi^{(2)} - \Pi$ and similarly for the other variables, (6.17) can be rewritten as

$$\kappa(\Pi+\Pi')(\theta_{\rm v}+\theta_{\rm v}')(\rho+\rho') = \frac{p+p'}{c_p}. \quad (6.18)$$

Using the definition of Π,

$$\Pi^{(2)} \equiv \Pi + \Pi' = \left(\frac{p+p'}{p_0}\right)^{\kappa} = \left(\frac{p}{p_0}\right)^{\kappa}\left(1+\frac{p'}{p}\right)^{\kappa} \simeq \Pi\left(1+\frac{\kappa p'}{p}\right). \quad (6.19)$$

Replacing p' by $p\Pi'/\kappa\Pi$, expanding (6.18) and neglecting products of primed quantities, the following linearized form of the equation of state is obtained:

$$\kappa\Pi\overline{\theta_{\rm v}}^{r}\rho' + \left(\kappa\overline{\theta_{\rm v}}^{r}\rho - \frac{p}{\kappa c_p\Pi}\right)\Pi' + \kappa\Pi\rho\overline{\theta_{\rm v}'}^{r} = \frac{p}{c_p} - \kappa\Pi\overline{\theta_{\rm v}}^{r}\rho. \quad (6.20)$$

(*c*) *The elliptic boundary-value problem*

(6.6), (6.11)–(6.13), (6.15) and (6.20) constitute a linear, coupled set of implicit equations for the variables $\theta^{(2)}$, $u^{(2)}$, $v^{(2)}$, $w^{(2)}$, $\rho^{(2)}$ and $\Pi^{(2)} \equiv \Pi^{n+1}$. The equations are solved by writing them as a single equation in one unknown, $\Pi' \equiv \Pi^{(2)} - \Pi$.

In order to do this, several steps first need to be followed. Specifically, explicit equations for the primed variables, including ρ' and $\theta_{\rm v}'$, need to be derived.

(i) *Potential temperature.* (6.6) can be rewritten as

$$\theta' \equiv \theta^{(2)} - \theta = (\theta^{(1a)} - \theta) - \alpha_2 \Delta t w' \delta_{2r} \theta_{\rm ref}, \tag{6.21}$$

where $w' \equiv w^{(2)} - w$.

(ii) *Virtual potential temperature.* Using (3.2) and $\theta_{\rm v} \equiv T_{\rm v}/\Pi$, with $\theta^{(2)}$ and $m_X^{(2)}$ as estimates for θ and m_X, leads to

$$\theta_{\rm v}' \equiv \theta_{\rm v}^{(2)} - \theta_{\rm v} = (\theta' + \theta) \left(\frac{1 + m_{\rm vap}^{(2)}/\epsilon}{1 + \sum_{X={\rm vap,cl,cf}} m_X^{(2)}} \right) - \theta_{\rm v}. \tag{6.22}$$

(iii) *Wind components.* In principle, expressions for $u' \equiv u^{(2)} - u$ and $v' \equiv v^{(2)} - v$ can be straightforwardly obtained from (6.11) and (6.12). However, in order to avoid an overly large numerical stencil, these equations are first rearranged semi-analytically to eliminate $v^{(2)}$ from (6.11) and $u^{(2)}$ from (6.12). This results in

$$\begin{aligned} u' \equiv u^{(2)} - u = A_u \left\{ R_u - \alpha_3 \Delta t \frac{c_p}{\overline{r}^{\lambda} \cos\phi} \left(\overline{\theta_{\rm v}^{(1a)}}^{r\lambda} \delta_\lambda \Pi' - \overline{\theta_{\rm v}^{(1a)} \delta_r \Pi'}^{r\lambda} \delta_\lambda r \right) \right\} \\ + F_u \left\{ \overline{R_v}^{\lambda\phi} - \alpha_3 \Delta t \overline{\frac{c_p}{\overline{r}^{\phi}} \left(\overline{\theta_{\rm v}^{(1a)}}^{r\phi} \delta_\phi \Pi' - \overline{\theta_{\rm v}^{(1a)} \delta_r \Pi'}^{r\phi} \delta_\phi r \right)}^{\lambda\phi} \right\}, \end{aligned} \tag{6.23}$$

$$\begin{aligned} v' \equiv v^{(2)} - v = A_v \left\{ R_v - \alpha_3 \Delta t \frac{c_p}{\overline{r}^{\phi}} \left(\overline{\theta_{\rm v}^{(1a)}}^{r\phi} \delta_\phi \Pi' - \overline{\theta_{\rm v}^{(1a)} \delta_r \Pi'}^{r\lambda} \delta_\phi r \right) \right\} \\ - F_v \left\{ \overline{R_u}^{\lambda\phi} - \alpha_3 \Delta t \overline{\frac{c_p}{\overline{r}^{\lambda} \cos\phi} \left(\overline{\theta_{\rm v}^{(1a)}}^{r\lambda} \delta_\lambda \Pi' - \overline{\theta_{\rm v}^{(1a)} \delta_r \Pi'}^{r\lambda} \delta_\lambda r \right)}^{\lambda\phi} \right\}, \end{aligned} \tag{6.24}$$

where

$$R_u \equiv (u^{(1)} - u) - \alpha_3 \Delta t \frac{c_p}{\overline{r}^{\lambda} \cos\phi} \left\{ \overline{(\theta_{\rm v}^{(1a)} - \theta_{\rm v})}^{r\lambda} \delta_\lambda \Pi - \overline{(\theta_{\rm v}^{(1a)} - \theta_{\rm v}) \delta_r \Pi}^{r\lambda} \delta_\lambda r \right\}, \tag{6.25}$$

$$R_v \equiv (v^{(1)} - v) - \alpha_3 \Delta t \frac{c_p}{\overline{r}^{\phi}} \left\{ \overline{(\theta_{\rm v}^{(1a)} - \theta_{\rm v})}^{r\phi} \delta_\phi \Pi - \overline{(\theta_{\rm v}^{(1a)} - \theta_{\rm v}) \delta_r \Pi}^{r\phi} \delta_\phi r \right\}, \tag{6.26}$$

$$A_u = \frac{1}{(1 + \alpha_3^2 f_r^2 \Delta t^2)}, \qquad F_u = \alpha_3 \Delta t f_r A_u. \tag{6.27}$$

A_v and F_v have the same form as A_u and F_u respectively but the f_r terms are evaluated at v-points rather than u-points.

(6.13) is rearranged into the form

$$w' \equiv w^{(2)} - w = G^{-1} R_w - K \delta_r \Pi', \tag{6.28}$$

where

$$R_w \equiv (w^{(1)} - w) - \alpha_4 c_p \Delta t (\theta_v^{(1a)} - \theta_v)\delta_r \Pi, \tag{6.29}$$

and

$$K \equiv \frac{\alpha_4 \Delta t c_p \theta_v^{(1a)}}{G}. \tag{6.30}$$

(iv) *Dry density.* (6.15) is rearranged as

$$\begin{aligned}\rho'_{\rm dry} \equiv \rho^{(2)}_{\rm dry} - \rho_{\rm dry} = -\frac{\Delta t}{r^2 \delta_\eta r}\Bigg[& \frac{1}{\cos\phi}\delta_\lambda \left\{ \frac{\overline{r^2 \rho_{\rm dry}\delta_\eta r}^{\lambda}}{\overline{r}^{\lambda}} (u + \alpha_1 u') \right\} \\ & + \frac{1}{\cos\phi}\delta_\phi \left\{ \frac{\overline{r^2 \rho_{\rm dry}\delta_\eta r}^{\phi}}{\overline{r}^{\phi}} (v + \alpha_1 v')\cos\phi \right\} \\ & - \delta_\eta \left\{ \overline{r^2\rho_{\rm dry}}^{r} \left(\frac{\overline{\overline{(u+\alpha_1 u')}^{\eta}}^{\lambda}}{\overline{r}^{\lambda}\cos\phi}\delta_\lambda r + \frac{\overline{\overline{(v+\alpha_1 v')}^{\eta}}^{\phi}}{\overline{r}^{\phi}}\delta_\phi r \right) \right\} \\ & + \delta_\eta \{ \overline{r^2\rho_{\rm dry}}^{r} (w + \alpha_2 w') \} \Bigg]. \end{aligned} \tag{6.31}$$

(v) *Moist density.* From (3.1) the estimate $\rho^{(2)}$ for ρ^{n+1} is defined by

$$\rho^{(2)} \equiv \rho^{(2)}_{\rm dry} \overline{\left(1 + \sum_{X={\rm vap,cl,cf}} m_X^{(2)} \right)}^{r}, \tag{6.32}$$

from which it follows that

$$\rho' \equiv \rho^{(2)} - \rho = \rho'_{\rm dry} \overline{\left(1 + \sum_{X={\rm vap,cl,cf}} m_X^{(2)} \right)}^{r} + \rho_{\rm dry} \left(\sum_{X={\rm vap,cl,cf}} \overline{(m_X^{(2)} - m_X)}^{r} \right). \tag{6.33}$$

(vi) *Derivation and solution of the elliptic equation.* Substituting (6.22) and (6.33) into (6.20), and using (6.21), (6.23), (6.24), (6.28) and (6.31) to algebraically eliminate the unknown quantities θ', u', v', w' and $\rho'_{\rm dry}$ respectively, results in (B.1), an equation for Π' which is linear, has variable coefficients and is elliptic provided $G > 0$. Since $\delta_r \Pi$ is always less than zero for all realistic scenarios, G can only be less than unity if $\delta_{2r}\theta_{\rm ref} < 0$, i.e. if the model atmosphere becomes statically unstable. In extreme cases the static instability may be sufficient to make $G \leq 0$. To avoid this the value that G can take is limited to $G_{\rm tol}$ which results in a limit on $\delta_{2r}\theta_{\rm ref}$ as in (6.7). Further details on the elliptic equation are presented in appendix B.

(B.1) is solved efficiently using a generalized conjugate residual (GCR) iterative solver (Eisenstat *et al.* 1983; Smolarkiewicz and Margolin 1994) and appropriate preconditioners. In LAM configurations, where the horizontal grid is nearly uniform, preconditioning in the vertical is sufficient. In global configurations, the decrease in longitudinal grid-spacing towards the poles leads to an increase in the condition number

and a large number of iterations being required to achieve a sufficiently converged solution. The iterations are reduced by using a two-dimensional alternating-direction-implicit (ADI) preconditioner (Skamarock *et al.* 1997) in the vertical and longitudinal directions.

(vii) *Back substitution and completion of the time step.* Once (B.1) has been solved for Π', $\Pi^{n+1} \equiv \Pi^{(2)}$ is obtained and the estimators $u^{(2)}$, $v^{(2)}$ and $w^{(2)}$ are evaluated by back substitution of Π' into (6.23), (6.24) and (6.28). Next the resulting values of u', v' and w' are used, together with Π', to obtain $\theta^{(2)}$ and $\rho_{\mathrm{dry}}^{(2)} \equiv \rho_{\mathrm{dry}}^{n+1}$ from (6.21) and (6.31), respectively. Now that $\rho_{\mathrm{dry}}^{n+1}$ is known, conservation of any of the quantities m_X (and any other passive tracer), θ and the three wind components is achieved by applying the Priestley (1993) scheme. This uses a combination of linear and higher-order interpolation estimates to obtain the desired conservation. Monotonicity, if desired, is similarly obtained using the Bermejo and Staniforth (1992) scheme. The resulting estimates for m_X, any passive tracers, θ and the three wind components are the final ones and they become the values of the variables at time step $n + 1$. If no conservation or monotonicity is applied then $m_X^{n+1} \equiv m_X^{(2)}$ and similarly for the other variables.

(*d*) *Other considerations*

A suitable choice for the time step is given by setting $C \equiv U\Delta t/\Delta \simeq 0.3$ where C is a measure of the Courant number (typically, explicit schemes require $C < 1$ everywhere for stability and usually $C \simeq 0.25$ for accuracy), Δ is a measure of the grid size and U is an appropriate estimate of the wind speed. This choice of value for C results in $\Delta t \simeq 30$ s when $\Delta = 1000$ m and $U = 10$ m s^{-1}. Note that this would imply a Courant number for the fastest (external) gravity wave which is greater than 10 and which would be far beyond the stability limit for an explicit scheme. In the configurations run at the Met Office, the vertical resolution does not change much and is typically around 300 m at an altitude of 1 km whereas horizontal resolutions vary from 1 km to 300 km. In practice, the physics parametrizations limit the time step since they have explicit time stepping within their numerics. It may also be necessary to adjust the time step to allow for an integral number of time steps per post-processing time interval (which is typically one hour). The time steps used at 1 km and 300 km horizontal resolutions are typically 30 s and 1800 s respectively. At high horizontal resolution it is possible to run successfully with longer time steps than indicated by the above to reduce the run-time. This is likely to be successful provided the average wind speed is not too strong. However, if the time step is increased too much, so that the Courant number also increases, the iteration count in the elliptic solver tends to increase, which offsets some of the efficiency gain. It also increases the time truncation error.

An increase in the Courant number may also arise in global configurations where the longitudinal grid length decreases towards the poles and the iteration count of the elliptic solver increases solely because of slower convergence of the solution near to the poles. This increase in iterations is reduced by applying a filter based on a conservative horizontal diffusion operator in spherical coordinates in the longitudinal direction only. When applied to a field X (θ, u, v or w) the discretized operator has the form

$$\mathrm{D}(X) = \left(\frac{1}{4r^2\delta_\eta r}\right) \Delta\lambda\delta_\lambda\{r^2\Delta\lambda\delta_\lambda(X\delta_\eta r)\}. \tag{6.34}$$

The operator eliminates two-grid-length waves and heavily damps other short wavelengths. The damping of the shorter waves is increased by multiple application of the filter. It is applied where the longitudinal grid length is at least an order of magnitude smaller than the grid length at the equator.

7. RESULTS

The new scheme has undergone a wide range of testing. There is space in this paper only to give a brief summary and a few examples of the tests; more complete results of the tests will be published elsewhere.

Before the full model was tested, many tests were conducted to evaluate individual components of the scheme and to clarify design issues. Tests to confirm the desirability of using the Charney–Phillips staggering in the vertical and to ensure that the boundary-layer parametrization worked properly with this staggering were reported in Cullen *et al.* (1997). Shallow water tests (Williamson *et al.* 1992) were conducted by Malcolm (1996) using a shallow water version of the scheme and these confirmed that the new scheme was superior to the split-explicit version of the UM.

A two-dimensional (longitudinal and vertical) slice version of the model (without physics) has been used for parameter and algorithmic testing in controlled environments, e.g. idealized two-dimensional flow over orography (Smith 1980; Pinty *et al.* 1995; Héreil and Laprise 1996; Ólafsson and Bougeault 1996). Similar types of tests may also be run in three dimensions without orography (Held and Suarez 1994) or with simplified orography (Qian *et al.* 1998). An idealized version of the model with a simplified representation of the Himalayas was used to test alternative flattening criteria for the vertical grid over orography. The various test configurations continue to be used in testing and evaluating changes.

However well a scheme performs in controlled test environments, the crucial test is how it performs as part of a full NWP or climate model. Validation is ultimately against observation (or analysis) since there are no realistic exact solutions. Much of the skill of the full model depends upon the quality of the physics parametrizations and, additionally for NWP, the data assimilation system, neither of which are addressed in this paper. Most of the physics parametrizations have also been upgraded. The new physics package was trialled in the old dynamical core but the model performance was worsened overall, even with increased vertical resolution which was needed to get the best out of the new physics. The combination of the new dynamical core and new physics is better overall than the old dynamical core with either new or old physics but its tropical performance is slightly worse. The full model with a complete physics package has undergone a lengthy period of pre-operational testing for both NWP and climate modelling.

To test the new scheme in NWP, the Met Office variational data assimilation scheme (VAR, Lorenc *et al.* (2000)) was coupled to the model, and VAR trials (continuous periods of data assimilation and forecasts) conducted. The longitudinal spacing of the model was 1.25° (288 intervals around a latitude circle), the latitudinal spacing was 0.833° (216 intervals between the poles) and there were 38 levels in the vertical. Initially these tests were for fixed periods and compared against the then-operational model as a control for the same period. Once the new system had reached an acceptable standard, a parallel trial against the operational system was begun (almost in real time and using the same data cut-off times). The trialling system used the same verification as the routine operational system. The verification system calculates a wide range of scores for various fields, e.g. r.m.s. (root-mean-square) of differences between forecasts and either observations or verifying analyses. A selection of these scores, chosen to reflect the forecast skill requirements across a range of forecast products, are combined to form an index value which is used routinely to give an overall indication of the skill of the forecast system in use at the Met Office (the 'NWP index'). However, the individual components of the index and a wider range of measures together with climatological maps were used to evaluate model errors and to assess forecast skill.

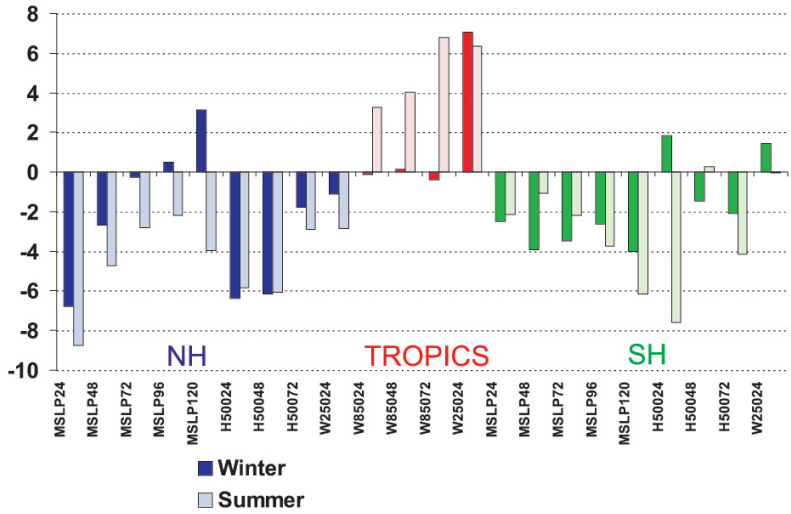

Figure 1. NWP index components comparing old and new UM. Northern hemisphere in blue, southern hemisphere in green and tropics in red. Light colouring are summer values, darker colouring winter. See text for further details.

Figure 1 shows a comparison of the NWP index components between the then-operational scheme and the new scheme from VAR trials for both winter (dark bars) and summer (light bars). The extra-tropical index components are MSLP (mean-sea-level pressure) daily to day 5, 500 hPa height daily to day 3 and T+24 250 hPa wind. The bars are coloured blue for northern hemisphere and green for the southern hemisphere. In the tropics (red bars) the components are 850 hPa wind daily to day 3 and T+24 250 hPa wind. Bars below the line are an indication that the new model is better. The new scheme is better overall outside the tropics, but worse in the tropics. However, tropical cyclone forecasts (not shown) were improved and the intensities of the cyclones were better maintained during the forecast.

During winter trial periods the new scheme was seen to be consistently better in the forecasting of major storms. An example taken from one of the trials is shown in Fig. 2. The two depressions shown gave severe weather across France and neighbouring countries on 26 and 27 December 1999. The MSLP analysis (lower panels) show the first storm over Germany and the second approaching north-west France. The middle panels show the then-operational 4 and 5-day forecasts which fail to capture either storm adequately. The upper panels shows the same forecasts for the new model which are considerably better.

The new scheme is also used for mesoscale modelling, and a 12 km horizontal resolution version for the UK is run four times a day. This also underwent pre-operational trials in parallel with the operational model. The performance of the mesoscale model is routinely assessed by comparing the model against observations of 1.5 m (screen) temperature and relative humidity, 10 m wind, visibility, cloud cover and precipitation. In the trial, the new version verified slightly better for all quantities apart from precipitation during the early part of the forecast. Case-studies using very high vertical and horizontal resolutions have already demonstrated the usefulness of running the model at high resolution for precipitation forecasts (Lean and Clark 2003) and in diagnostic studies of mesoscale phenomena (Clark *et al.* 2005).

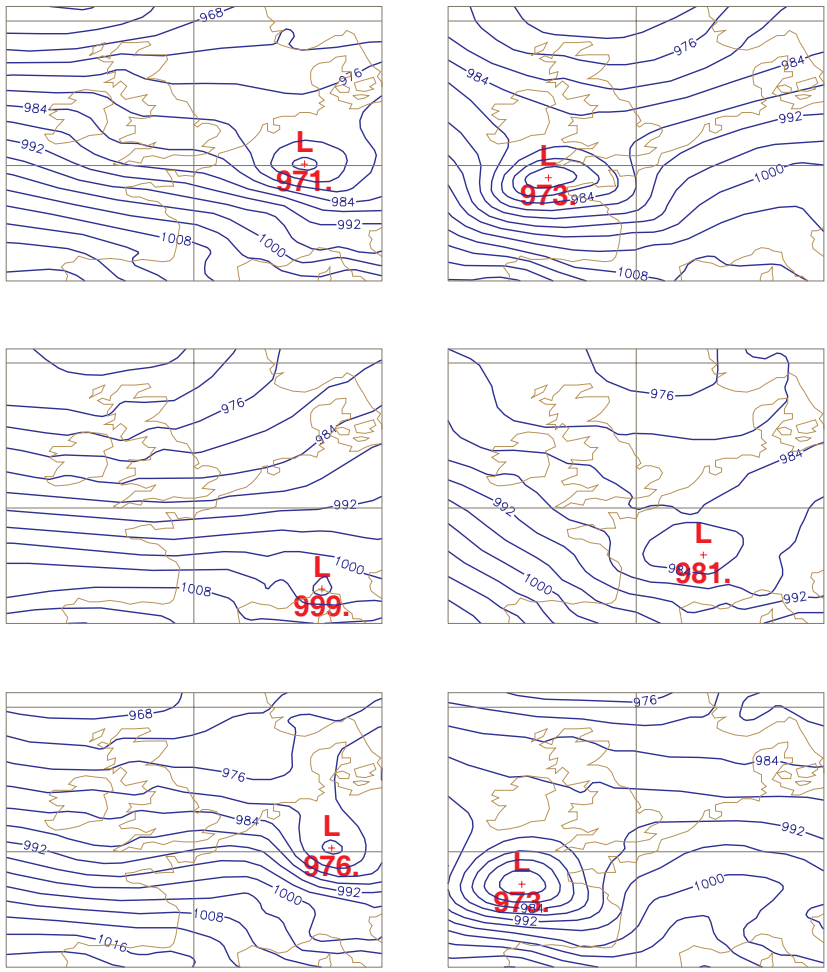

Figure 2. MSLP for 12 UTC 26 December 1999 (left column) and 12 UTC 27 December 1999 (right column). Top frames are 4-day (left) and 5-day (right) forecasts from new scheme. Middle frames are corresponding forecasts from old model. Lower frames are verifying analyses.

Climate tests of the new model were made, initially for one season or one year and then extending these to several years AMIP runs using observed sea surface temperatures (AMIP is the Atmospheric Model Intercomparison Project, see Gates (1992)). Validation of a climate model involves checking that it can reproduce the observed climate derived from re-analyses (NCEP–NCAR: Kalnay *et al.* (1996); ECMWF: Gibson *et al.* (1997)), or obtained from satellites (e.g. Earth Radiation Budget Experiment (ERBE): Barkstorm *et al.* (1989)) or from conventional observations (e.g. the precipitation climatology of Xie and Arkin (1997)). The observed and modelled climatologies used are usually seasonal averages derived from at least several years of data. A wide range of features is assessed together with suitable measures of variability to ensure that the model has realistic variability. Taylor diagrams (Gates *et al.* 1999; Taylor 2001) are used to compare the standard deviation and r.m.s. differences between observed or analysed climatologies and models. Results from AMIP runs were compared against those

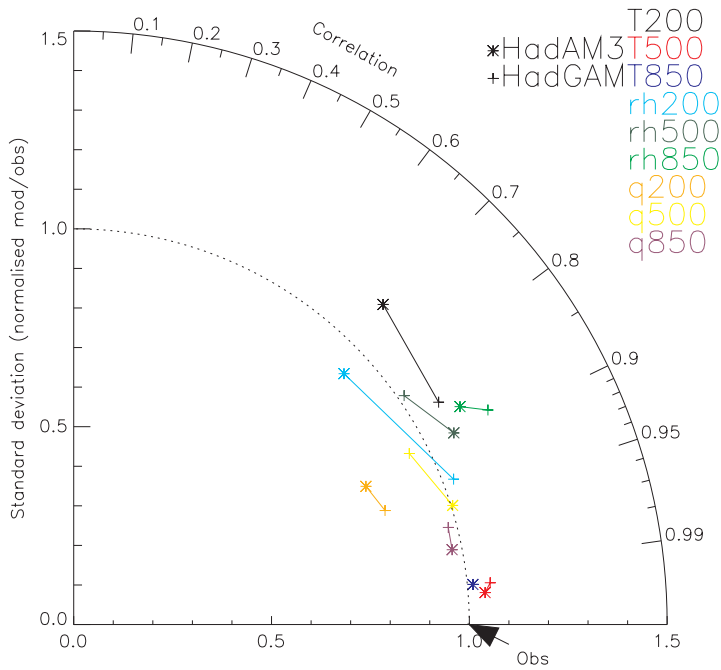

Figure 3. Taylor diagram for selected thermodynamic variables comparing old (HadAM3) and new (HadGAM) climate models. See text for details.

obtained from the best version of the climate model based on the old dynamical core (i.e. HadAM3, Hadley Centre Atmospheric Model, version 3). The longitudinal spacing of the model was 3.75° (96 intervals around a latitude circle), the latitudinal spacing was 2.5° (72 intervals between the poles) and there were 19 levels in the vertical. As indicated above, better performance of this model has not been achieved with either increased vertical resolution or new physics. The new model (HadGAM, Hadley Centre Global Atmospheric Model) was run with the same horizontal resolution but with 38 levels in the vertical.

Figure 3 shows a Taylor diagram comparing the old (HadAM3, $*$ points) and new (HadGAM, $+$points) climate models for a selection of temperature and moisture fields. Points on the unit radius have the same standard deviation as observed. Points nearer the horizontal axis have smaller r.m.s. differences from observed. Overall the new model is better due to the larger beneficial changes at upper levels. Other plots (not shown) show both positive and negative impacts but overall the new model is considered to be better.

8. Conclusions

The current status of the dynamical core of the Met Office UM has been described. The new dynamical core solves the fully compressible, non-hydrostatic, deep-atmosphere equations. These are discretized using a predictor–corrector approach for a two-time-level SI SL scheme. Being non-hydrostatic, the new UM is now capable of NWP at very high resolution and has already delivered improved skill in both NWP and climate modelling.

The new UM has been operational in NWP since late 2002. It is used for global forecasting up to 6 days ahead, for UK mesoscale forecasts (12 km horizontal resolution up to 2 days ahead) and to provide high-resolution LAM forecasts anywhere in the world. Trials of LAMs at horizontal resolutions below 5 km are ongoing, and operational use at these resolutions will begin when computer resources become available. The climate version (HadGEM1, Hadley Centre Global Environmental Model which also includes improvements to the ocean and sea-ice models) is being used for climate change investigations.

ACKNOWLEDGEMENTS

Jon James and Susan Coulter took part in the development of early model versions. Chris Smith ran several test problems and their evaluation led to improvements in the formulation of the model. Piotr Smolarkiewicz suggested using the generalised conjugate residual scheme for the solver. Sean Milton supplied Fig. 1 and Gill Martin supplied Fig. 3. Many Met Office scientists were involved in bringing the new version of the UM to operational status.

APPENDIX A

Rotated grid

For a general latitude–longitude grid with the rotated pole situated at (λ_0, ϕ_0) in geographical coordinates, the Coriolis terms are

$$f_\lambda = -2\Omega \sin\lambda \cos\phi_0, \tag{A.1}$$

$$f_\phi = 2\Omega(\cos\phi \sin\phi_0 - \sin\phi \cos\lambda \cos\phi_0), \tag{A.2}$$

$$f_r = 2\Omega(\sin\phi \sin\phi_0 + \cos\phi \cos\lambda \cos\phi_0). \tag{A.3}$$

Thus for the coordinate pole coincident with the north pole $\phi_0 = \pi/2$, $f_r = 2\Omega \sin\phi$, $f_\phi = 2\Omega \cos\phi$ and $f_\lambda = 0$.

The actual horizontal wind components (u_A, v_A) at position (λ_A, ϕ_A) on the geographical grid are related to the horizontal wind components (u, v) at position (λ, ϕ) on the rotated grid through

$$u_A = u \cos\tau - v \sin\tau, \tag{A.4}$$

$$v_A = u \sin\tau + v \cos\tau, \tag{A.5}$$

where

$$\cos\tau = -\sin(\lambda_A - \lambda_0) \sin\lambda \sin\phi_0 - \cos(\lambda_A - \lambda_0) \cos\lambda, \tag{A.6}$$

$$\sin\tau = \sin(\lambda_A - \lambda_0)\frac{\cos\phi_0}{\cos\phi}, \tag{A.7}$$

and λ and ϕ are related to λ_A and ϕ_A by

$$\cos\phi \cos\lambda = -\cos(\lambda_A - \lambda_0) \cos\phi_A \sin\phi_0 + \sin\phi_A \cos\phi_0, \tag{A.8}$$

$$\cos\phi \sin\lambda = -\sin(\lambda_A - \lambda_0) \cos\phi_A, \tag{A.9}$$

$$\sin\phi = \sin\phi_A \sin\phi_0 + \cos(\lambda_A - \lambda_0) \cos\phi_A \cos\phi_0. \tag{A.10}$$

APPENDIX B

Elliptic equation

The elliptic equation resulting from the discretization of the model's equations is of a Helmholtz type and can be written as:

$$\begin{aligned} H(\Pi') \equiv{}& \frac{\Delta\lambda}{\cos\phi}\delta_\lambda(C_{xx1}X) + \frac{\Delta\phi}{\cos\phi}\delta_\phi(C_{yy1}Y) \\ &+ \delta_\eta\left\{C_{zz}\delta_\eta\Pi' - C_5\left(\overline{C_{xz}\overline{X}^{\eta}}^{\lambda} + \overline{C_{yz}\overline{Y}^{\eta}}^{\phi}\right)\right\} + C_3\overline{C_z\delta_\eta\Pi'}^{r} - C_4(\Pi') \\ ={}& \text{r.h.s.}, \end{aligned} \tag{B.1}$$

where

$$X = C_{xx2}\left(\Delta\lambda\delta_\lambda\Pi' - C_{xp}\overline{C_2\delta_r\Pi'}^{r\lambda}\right) + C_{xy1}\overline{C_{xy2}\left(\Delta\phi\delta_\phi\Pi' - C_{yp}\overline{C_2\delta_r\Pi'}^{r\phi}\right)}^{\lambda\phi}, \tag{B.2}$$

$$Y = C_{yy2}\left(\Delta\phi\delta_\phi\Pi' - C_{yp}\overline{C_2\delta_r\Pi'}^{r\phi}\right) - C_{yx1}\overline{C_{yx2}\left(\Delta\lambda\delta_\lambda\Pi' - C_{xp}\overline{C_2\delta_r\Pi'}^{r\lambda}\right)}^{\lambda\phi}, \tag{B.3}$$

$$C_{xx1} = \frac{\overline{r^2\rho_{\text{dry}}\delta_\eta r}^{\lambda}}{\overline{r}^{\lambda}\Delta\lambda}, \quad C_{xx2} = \alpha_1\alpha_3 A_u \Delta t c_p \overline{\theta_{\text{v}}^{(1a)}}^{r\lambda}, \tag{B.4}$$

$$C_{yy1} = \frac{\cos\phi\overline{r^2\rho_{\text{dry}}\delta_\eta r}^{\phi}}{\overline{r}^{\phi}\Delta\phi}, \quad C_{yy2} = \frac{\alpha_1\alpha_3 A_v \Delta t c_p \overline{\theta_{\text{v}}^{(1a)}}^{r\phi}}{\overline{r}^{\phi}\Delta\phi}, \tag{B.5}$$

$$C_{zz} = \frac{\alpha_2 K\overline{r^2\rho_{\text{dry}}}^{r}}{\delta_\eta r}, \quad C_z = \frac{\alpha_2 K\delta_{2r}\theta_{\text{ref}}}{\delta_\eta r}\left(\frac{1 + m_{\text{vap}}^{(2)}/\epsilon}{1 + \sum_{X=(\text{vap,cl,cf})} m_X^{(2)}}\right), \tag{B.6}$$

$$C_{xz} = \frac{\delta_\lambda r}{\overline{r}^{\lambda}\cos\phi}, \quad C_{yz} = \frac{\delta_\phi r}{\overline{r}^{\phi}}, \quad C_{xp} = \frac{\Delta\lambda\delta_\lambda r}{\overline{\theta_{\text{v}}^{(1a)}}^{r\lambda}}, \quad C_{yp} = \frac{\Delta\phi\delta_\phi r}{\overline{\theta_{\text{v}}^{(1a)}}^{r\phi}}, \tag{B.7}$$

$$C_{xy1} = \alpha_1\alpha_3\Delta t F_u, \quad C_{xy2} = c_p\overline{\theta_{\text{v}}^{(1a)}}^{r\phi}, \quad C_{yx1} = \alpha_1\alpha_3\Delta t F_v, \quad C_{yx2} = \frac{c_p\overline{\theta_{\text{v}}^{(1a)}}^{r\lambda}}{\overline{r}^{\lambda}\cos\phi\Delta\lambda}, \tag{B.8}$$

$$C_2 = \theta_{\text{v}}^{(1a)}, \quad C_3 = \frac{r^2\rho\delta_\eta r}{\overline{\theta_{\text{v}}}^{r}\left(1 + \sum_{X=(\text{vap,cl,cf})}\overline{m_X^{(2)}}^{r}\right)}, \tag{B.9}$$

$$C_4 = \frac{\delta_\eta r\left(\dfrac{r^2 p}{R_{\text{dry}}\Pi} - \kappa r^2\rho\overline{\theta_{\text{v}}}^{r}\right)}{\kappa\Delta t\Pi\overline{\theta_{\text{v}}}^{r}\left(1 + \sum_{X=(\text{vap,cl,cf})}\overline{m_X^{(2)}}^{r}\right)}, \quad C_5 = \overline{r^2\rho_{\text{dry}}}^{r}, \tag{B.10}$$

$$
\begin{aligned}
\text{r.h.s.} = &- \frac{\delta_\eta r\left(\kappa r^2 \rho \Pi \overline{\theta_{\mathrm{v}}^{(1a)}}^{r} - r^2 p/c_p\right)}{\Delta t \kappa \Pi \overline{\theta_{\mathrm{v}}}^{r}\left(1 + \sum_{X=(\mathrm{vap,cl,cf})} \overline{m_X^{(2)}}^{r}\right)} \\
&- \frac{r^2 \rho \delta_\eta r}{\Delta t\left(1 + \sum_{X=(\mathrm{vap,cl,cf})} \overline{m_X}^{r}\right)} \left(\frac{\sum_{X=(\mathrm{vap,cl,cf})} \overline{\left(m_X^{(2)} - m_X\right)}^{r}}{1 + \sum_{X=(\mathrm{vap,cl,cf})} \overline{m_X^{(2)}}^{r}} \right) \\
&+ \frac{\Delta\lambda}{\cos\phi}\delta_\lambda(C_{xx1}u_*) + \frac{\Delta\phi}{\cos\phi}\delta_\phi(C_{yy1}v_*) \\
&+ \delta_\eta\left\{C_5\left(\dot\eta \delta_\eta r + \alpha_2 G^{-1} R_w - \overline{C_{xz}\overline{(u_* - u)}^{\eta}}^{\lambda} - \overline{C_{yz}\overline{(v_* - v)}^{\eta}}^{\phi}\right)\right\} \\
&+ C_3 \overline{\left(\frac{1 + m_{\mathrm{vap}}^{(2)}/\epsilon}{1 + \sum_{X=(\mathrm{vap,cl,cf})} m_X^{(2)}}\right)(\alpha_2 \delta_{2r} \theta_{\mathrm{ref}} G^{-1} R_w)}^{r} \ , \qquad \text{(B.11)}
\end{aligned}
$$

$$
u_* = u + \alpha_1(A_u R_u + F_u \overline{R_v}^{\lambda\phi}), \quad v_* = v + \alpha_1(A_v R_v - F_v \overline{R_u}^{\lambda\phi}), \qquad \text{(B.12)}
$$

where R_u, R_v and R_w are defined in (6.25), (6.26) and (6.29), A_u, A_v, F_u and F_v are defined in (6.27), K in (6.30) and G in (6.14). Due to the singularity of the term $(1/\cos\phi)$ at the poles, the GCR(k) solves a modified system $H(\Pi')\cos\phi =$ r.h.s. $\cos\phi$.

REFERENCES

Arakawa, A. and Konor, C. S. 1996 Vertical differencing of the primitive equations based on the Charney–Phillips grid in hybrid σ–p vertical coordinates. *Mon. Weather Rev.*, **124,** 511–528

Arakawa, A. and Lamb, V. R. 1977 Computational design of the basic dynamical processes of the UCLA general circulation model. *Methods Comput. Phys.*, **17,** 173–265

Barkstorm, B., Harrison, E., Smith, G., Green, R., Kibler, J. and Cess, R. 1989 Earth Radiation Budget Experiment (ERBE) 1985 archival and April 1985 results. *Bull. Am. Meteorol. Soc.*, **70,** 1254–1262

Bates, J. R., Moorthi, S. and Higgins, R. W. 1993 A global multilevel atmospheric model using a vector semi-Lagrangian finite-difference scheme. Part 1: Adiabatic formulation. *Mon. Weather Rev.*, **121,** 244–263

Bermejo, R. and Staniforth, A. 1992 The conversion of semi-Lagrangian advection schemes to quasi-monotone schemes. *Mon. Weather Rev.*, **120,** 2622–2632

Clark, P. A., Browning, K. A. and Wang, C. 2005 The sting at the end of the tail: Model diagnostics of fine scale 3D structure of the cloud head. *Q. J. R. Meteorol. Soc.* (in press)

Côté, J., Gravel, S., Méthot, A., Patoine, A., Roch, M. and Staniforth, A. 1998 The operational CMC–MRB Global Environmental Multiscale (GEM) model. Part I: Design considerations and formulation. *Mon. Weather Rev.*, **126,** 1373–1395

Cullen, M. J. P. 1989 Implicit finite difference methods for modelling discontinuous atmospheric flows. *J. Comput. Phys.*, **81,** 319–348

1990 A test of a semi-implicit integration technique for a fully compressible non-hydrostatic model. *Q. J. R. Meteorol. Soc.*, **116,** 1253–1258

1999 'The use of dynamical knowledge of the atmosphere to improve NWP models'. Pp. 418–441 in ECMWF Seminar Proceedings: Recent developments in numerical methods for atmospheric modelling, ECMWF, Reading, UK

2001 Alternative implementations of the semi-Lagrangian semi-implicit schemes in the ECMWF model. *Q. J. R. Meteorol. Soc.*, **127,** 2787–2802

Cullen, M. J. P. and Davies, T. 1991 A conservative split-explicit integration scheme with fourth-order horizontal advection. *Q. J. R. Meteorol. Soc.*, **117,** 993–1002

Cullen, M. J. P., Norbury, J., Purser, R. J. and Shutts, G. J. 1987 Modelling the quasi-equilibrium dynamics of the atmosphere. *Q. J. R. Meteorol. Soc.*, **113,** 735–757

Cullen, M. J. P., Davies, T., Mawson, M. H., James, J. A., Coulter, S. C. and Malcolm, A. 1997 'An overview of numerical methods for the next generation UK NWP and climate model'. Pp. 425–444 in *Numerical Methods in Atmosphere and Ocean Modelling, The André Robert memorial volume*, Eds. C. Lin, R. Laprise and H. Ritchie. Canadian Meteorological and Oceanographical Society, Ottawa, Canada

Davies, T., Staniforth, A., Wood, N. and Thuburn, J. 2003 Validity of anelastic and other equation sets as inferred from normal-mode analysis. *Q. J. R. Meteorol. Soc.*, **129,** 2761–2775

Eisenstat, S. C., Elman, H. C. and Schultz, M. H. 1983 Variational iterative methods for nonsymmetric systems of linear equations. *SIAM J. Numer. Anal.*, **20,** 345–357

Fureby, C. and Grinstein, F. F. 2002 Large eddy simulation of high-Reynolds-number free and wall-bounded flows. *J. Comput. Phys.*, **181,** 68–97

Gates, W. L. 1992 AMIP: the Atmospheric Model Intercomparison Project. *Bull. Am. Meteorol. Soc.*, **73,** 1962–1970

Gates, W. L., Boyle, J. S., Covey, C., Dease, C. G., Doutriaux, C. M., Drach, R. S., Fiorino, M., Gleckler, P. J., Hnilo, J. J., Marlais, S. M., Phillips, T. J., Potter, G. L., Santer, B. D., Sperber, K. R., Taylor, K. E. and Williams, D. N. 1999 An overview of the results of the Atmospheric Model Intercomparison Project (AMIP I). *Bull. Am. Meteorol. Soc.*, **80,** 29–55

Gibson, J., Kållberg, P., Uppala, S., Hernandez, A., Nomura, A. and Serrano, E. 1997 ERA-15 description. *ECMWF Re-analysis Project Report Series*, **1,** 1–74

Gill, A. E. 1982 *Atmosphere–ocean dynamics*, 1st edn. Academic Press, London

Golding, B. W. 1992 An efficient non-hydrostatic forecast model. *Meteorol. Atmos. Phys.*, **50,** 89–103

Held, I. M. and Suarez, M. J. 1994 A proposal for the intercomparison of dynamical cores of atmospheric general circulation models. *Bull. Am. Meteorol. Soc.*, **75,** 1825–1830

Héreil, P. and Laprise, R. 1996 Sensitivity of internal gravity waves solutions to time step of a semi-implicit semi-Lagrangian nonhydrostatic model. *Mon. Weather Rev.*, **124,** 972–999

Kálnay de Rivas, E. 1972 On the use of nonuniform grids in finite-difference equations. *J. Comput. Phys.*, **10,** 202–210

Kalnay, E., Kanamitsu, M., Kistler, R., Collins, W., Deaven, D., Gandin, L., Iredell, M., Saha, S., White, G., Woollen, J., Zhu, Y., Leetmaa, A., Chelliah, M., Ebisuzaki, W., Higgins, W., Janowiak, J., Mo, K. C., Ropelewski, C., Wang, J., Jenne, R. and Joseph, D. 1996 The NCEP/NCAR 40-year reanalysis project. *Bull. Am. Meteorol. Soc.*, **77,** 437–471

Lean, H. W. and Clark, P. A. 2003 The effects of changing resolution on mesoscale modelling of line convection and slantwise circulation in FASTEX IOP16. *Q. J. R. Meteorol. Soc.*, **129,** 2255–2278

Lions, J.-L., Teman, R. and Wang, S. 1992a New formulations of the primitive equations of atmosphere and applications. *Nonlinearity*, **5,** 237–288

1992b On the equations of the large-scale ocean. *Nonlinearity*, **5,** 1007–1053

Lorenc, A. C., Ballard, S. P., Bell, R. S., Ingleby, N. B., Andrews, P. L. F., Barker, D. M., Bray, J. R., Clayton, A. M., Dalby, T., Li, D., Payne, T. J. and Saunders, F. W. 2000 The Met. Office global three-dimensional variational data assimilation scheme. *Q. J. R. Meteorol. Soc.*, **126,** 2991–3012

Malcolm, A. J. 1996 'Evaluation of the proposed new Unified Model scheme versus the current Unified Model scheme on the shallow water equations'. Met Office FR Technical Note No. 180

McDonald, A. and Bates, J. R. 1989 Semi-Lagrangian integration of a gridpoint shallow water model on the sphere. *Mon. Weather Rev.*, **117,** 130–137

Ólafsson, H. and Bougeault, P. 1996 Nonlinear flow past an elliptic mountain ridge. *J. Atmos. Sci.*, **53,** 2465–2489

Oliger, J. and Sundström, A. 1978 Theoretical and practical aspects of some initial boundary value problems in fluid dynamics. *SIAM J. Appl. Math.*, **35,** 419–446

Phillips, N. A. 1957 A coordinate system having some special advantages for numerical forecasting. *J. Meteor.*, **14,** 184–185

Pinty, J.-P., Benoit, R., Richard, E. and Laprise, R. 1995 Simple tests of a semi-implicit semi-Lagrangian model on 2D mountain wave problems. *Mon. Weather Rev.*, **123,** 3042–3058

Priestley, A. 1993 A quasi-conservative version of the semi-Lagrangian advection scheme. *Mon. Weather Rev.*, **121,** 621–629

Qian, J.-H., Semazzi, F. H. M. and Scroggs, J. S. 1998 A global nonhydrostatic semi-Lagrangian atmospheric model with orography. *Mon. Weather Rev.*, **126,** 747–771

Ritchie, H., Temperton, C., Simmons, A., Hortal, M., Davies, T., Dent, D. and Hamrud, M. 1995 Implementation of the semi-Lagrangian method in a high-resolution version of the ECMWF forecast model. *Mon. Weather Rev.*, **123,** 489–514

Robert, A. 1969 'The integration of a spectral model of the atmosphere by the implicit method'. Pp. VII-19–VII-24 in Proceedings WMO/IUGG Symposium on Numerical Weather Prediction. Japan Meteorol. Agency

1981 A stable numerical integration scheme for the primitive meteorological equations. *Atmos.–Ocean*, **19,** 35–46

Simmons, A. J. and Burridge, D. M. 1981 An energy and angular-momentum conserving vertical finite-difference scheme and hybrid vertical coordinates. *Mon. Weather Rev.*, **109,** 758–766

Skamarock, W. C., Smolarkiewicz, P. K. and Klemp, J. B. 1997 Preconditioned conjugate-residual solvers for Helmholtz equations in nonhydrostatic models. *Mon. Weather Rev.*, **125,** 587–599

Smith, R. B. 1980 Linear theory of stratified hydrostatic flow past an isolated mountain. *Tellus*, **32,** 348–364

Smolarkiewicz, P. K. and Margolin, L. G. 1994 'Variational elliptic solver for atmospheric applications'. Technical Report LA-12712-MS, Los Alamos, USA

Staniforth, A. and Côté, J. 1991 Semi-Lagrangian integration schemes for atmospheric models—a review. *Mon. Weather Rev.*, **119,** 2206–2223

Staniforth, A., White, A., Wood, N., Thuburn, J., Zerroukat, M., Cordero, E. and Davies, T. 2004 'The Joy of U.M. 6.0—model formulation'. Unified Model Documentation Paper No. 15. Available online at http://www.metoffice.com/research/nwp/publications/papers/unified_model/index.html

Tanguay, M., Robert, A. and Laprise, R. 1990 A semi-implicit semi-Lagrangian fully compressible regional forecast model. *Mon. Weather Rev.*, **118,** 1970–1980

Tapp, M. C. and White, P. W. 1976 A non-hydrostatic mesoscale model. *Q. J. R. Meteorol. Soc.*, **102,** 277–296

Taylor, K. E. 2001 Summarizing multiple aspects of model performance in a single diagram. *J. Geophys. Res.*, **106,** 7183–7192

Temperton, C., Hortal, M. and Simmons, A. 2001 A two-time-level semi-Lagrangian global spectral model. *Q. J. R. Meteorol. Soc.*, **127,** 111–127

Thuburn, J., Wood, N. and Staniforth, A. 2002 Normal modes of deep atmospheres. I: Spherical geometry. *Q. J. R. Meteorol. Soc.*, **128,** 1771–1792

White, A. A. and Bromley, R. A. 1995 Dynamically consistent, quasi-hydrostatic equations for global models with a complete representation of the Coriolis force. *Q. J. R. Meteorol. Soc.*, **121,** 399–418

White, A. A., Hoskins, B. J., Roulstone, I. and Staniforth, A. 2005 Consistent approximate models of the global atmosphere: shallow, deep, hydrostatic, quasi-hydrostatic and non-hydrostatic. *Q. J. R. Meteorol. Soc.* (in press)

Williamson, D. L., Drake, J. B., Hack, J. J., Jakob, R. and Swarztrauber, P. N. 1992 A standard test set for numerical approximations to the shallow water equations in spherical geometry. *J. Comput. Phys.*, **102,** 211–224

Wood, N. and Staniforth, A. 2003 The deep-atmosphere Euler equations with a mass-based vertical coordinate. *Q. J. R. Meteorol. Soc.*, **129,** 1289–1300

Xie, P. and Arkin, P. A. 1997 Global precipitation: a 17-year monthly analysis based on gauge observations, satellite estimates, and numerical model outputs. *Bull. Am. Meteorol. Soc.*, **78,** 2539–2558

Yeh, K.-S., Côté, J., Gravel, S., Méthot, A., Patoine, A., Roch, M. and Staniforth, A. 2002 The CMC–MRB Global Environmental Multiscale (GEM) model. Part III: Nonhydrostatic formulation. *Mon. Weather Rev.*, **130,** 339–356